UAV icing: Experimental validation data for predicting ice shapes at low Reynolds numbers

Richard Hann[1,2], Nicolas Müller[2], Markus Lindner[1,2], and Joachim Wallisch[1,2]

1 Norwegian University of Science and Technology (NTNU), Department of Engineering Cybernetics, UAV Icing Lab, Trondheim, Norway.

2 UBIQ Aerospace. Trondheim, Norway.

Abstract

Icing is a severe hazard to aircraft and in particular to unmanned aerial vehicles (UAVs). One important activity to understand icing risks is the prediction of ice shapes with simulation tools. Nowadays, several icing computational fluid dynamic (CFD) models exist. Most of these methods have been originally developed for manned aircraft purposes at relatively high Reynolds numbers. In contrast, typical UAV applications experience Reynolds numbers an order of magnitude lower, due to the smaller airframe size and lower airspeeds. This work proposes a set of experimental ice shapes that can serve as validation data for ice prediction methods at low Reynolds numbers. Three ice shapes have been collected at different temperatures during an experimental icing wind tunnel campaign. The obtained ice shapes represent wet (glaze ice, −2 °C), mixed (−4 °C), and dry (rime ice, −10 °C) ice growth regimes. The Reynolds number is between Re=5.6…6.0×10^5, depending on the temperature. The ice shapes were digitized with structure-from-motion, a photogrammetric method that builds 3D models from 2D image sequences. In addition, ice weight measurements and ice density approximations are available. This validation dataset is used in the 2nd AIAA Ice Prediction Workshop (IPW) as a base case scenario. The IPW is a recurring activity that aims to compare different 3D icing CFD methods about their ability to predict ice shapes. Overall, this work is adding a much-needed validation case for low Reynolds number icing, which will aid in the verification and development of ice prediction models.

Introduction

The effects of icing on unmanned aerial vehicles (UAVs)[1], urban air mobility (UAM), and advanced air mobility (AAM) applications have been a growing concern in recent years [1, 2]. Most of these aircraft – especially UAVs – operate at substantially lower Reynolds numbers compared to manned aviation, typically in the range of Re=10^5–10^7 [2]. Adverse weather, particularly atmospheric in-flight icing, poses a severe hazard to these aircraft, limiting their operational envelope and flyability [3]. In fact, UAVs today are unable to fly in any potential icing conditions, which greatly limits their commercial and military useability [4, 5]. Therefore, understanding how icing affects these aircraft and developing mature ice protection systems for them is essential to unlocking the potential of these new technologies and markets. Accurately modeling the ice accretion process and predicting ice shapes with icing computational fluid dynamic (CFD) methods is a crucial component in achieving this goal [6, 7]. Despite an abundance of ice shape validation data, all of it has been obtained at high Reynolds numbers, highlighting the need for low Reynolds number validation cases [8]. This work proposes three such cases for validation, which will be used in the 2nd AIAA Ice Prediction Workshop (www.icepredictionworkshop.com). This workshop is intended to compare different icing CFD methods using experimental cases. The first workshop focused on icing on manned aircraft whereas the second workshop includes the low-speed cases that are presented in this paper.

Method

The experimental campaign has been conducted in the icing wind tunnel facilities of the VTT Technical Research Centre of Finland in Helsinki in the fall of 2022 [9]. The tunnel has a 3×3 spray bar system and a test section size of 700×700 mm (width × height) located in a large cold room, see Fig. 1. An RG-15 airfoil was mounted near the end of the test section on a mounting system with small side plates, see Fig. 2. The entire airfoil was situated inside the tunnel. All tests have been conducted at identical conditions, except for a variation of the temperature between −2 °C (glaze), −4 °C (mixed), and −10 °C (rime). Temperatures are measured as static temperatures and fluctuation of ± 0.1 °C. The test conditions are shown in Tab. 1. After ice accretion was completed, the leading edge of the test wing was removed and the ice shape was digitized with a structure-from-motion (SfM) method.
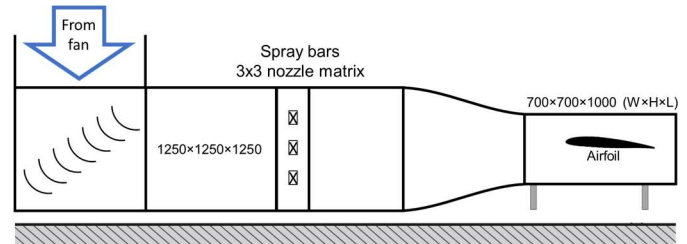

Figure 1. The general layout of the icing wind tunnel facilities, not to scale. The wind tunnel is located inside a large cold room.

---

[1] also called drones, remotely piloted aircraft systems (RPAS), unmanned aerial systems (UAS), uncrewed or unoccupied aerial vehicles.

Figure 3. The removable leading edge of the test wing with glaze ice (upper) and rime ice (lower) next to each other. The ice shapes have been trimmed to a width of 10 cm, as well as painted and powdered.
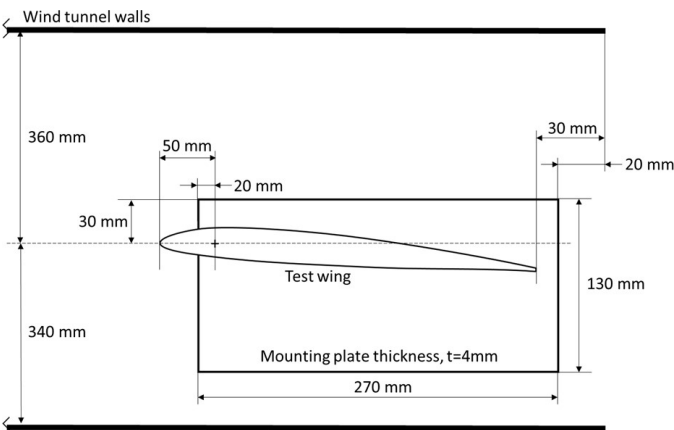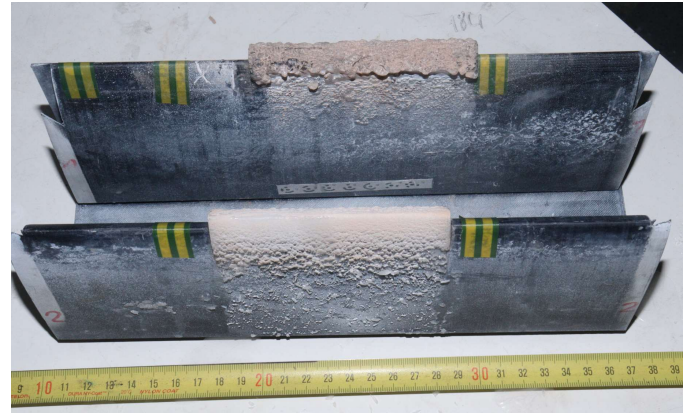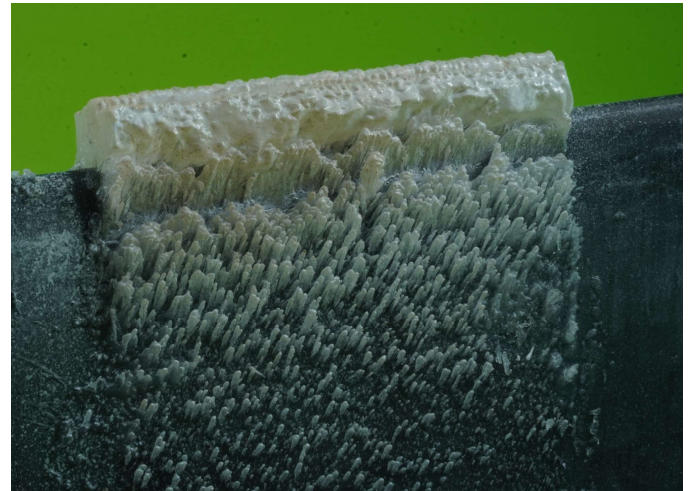

Figure 2. The wing is located inside the icing wind tunnel (top picture). Position and dimensions of the test wing and mounting plate in the icing wind tunnel, not to scale (bottom picture).

Figure 4. Closeup of the mixed ice shape after painting and powdering, ready for post-processing.

Test wing

The test wing is a rectangular wing with a chord length of 0.30 m and a span of 0.58 m. The wing is based on an RG-15 airfoil, which is a geometry that is often used for small UAV wings (e.g. [10]). The wing had a removable leading edge section with a width of 0.30 m in a spanwise direction and a chordwise depth of 0.10 m. The wing has been 3D printed in a thermoplastic polyester material, polylactic acid (PLA). The main body of the wing has been printed as three separate parts. The surface of the entire wing was sanded to ensure an aerodynamically smooth surface. The wing was mounted inside the wind tunnel, as indicated in the schematic of Fig. 2. After ice accretion, a hot metal plate was used to remove ice from the non-removable part of the leading edge. Then, the leading edge was carefully removed from the wing and processed further. Finally, the ice shape was further trimmed to a width of 0.10 m, for easier processing, see Fig. 3 and 4.

Table 1. Test case description

Airfoil	RG-15
Span	0.59 m
Chord	0.30 m
Airspeed	25 m/s
Angle of attack	+4°
Liquid water content (LWC)	0.44 g/m³
Median volume diameter (MVD)	23 microns
Duration	20 min
Static temperature (glaze, mixed, rime)	[−2, −4, −10]°C
Reynolds numbers	$[5.7, 5.8, 6.0] \times 10^5$
Relative Humidity	95–100%

Droplet size distribution

The droplet size distribution was determined in a previous study in the summer of 2018 [11], using an optical icing condition evaluation method (ICEMET) system [12, 13]. The ICEMET-sensor droplet size measurement range is between 5–200 μm and each bin size is 1 μm. The smallest bin class is 5–6 μm and bin sizes continue in the same way into the last bin class. The sensor was placed in the center of the

test section. The most representative droplet size distribution is considered to be obtained by averaging all Case 2 and Case 3 measurements from the study [11], and is shown in Fig. 5. The result is a 1-bin size MVD of 22.7 µm ± 1.5 µm, which is rounded to a nominal 1-bin MVD of 23 µm. A 7-bin distribution is recommended for simulations and is presented in Tab. 2.

Table 2. The 7-bin droplet distribution.

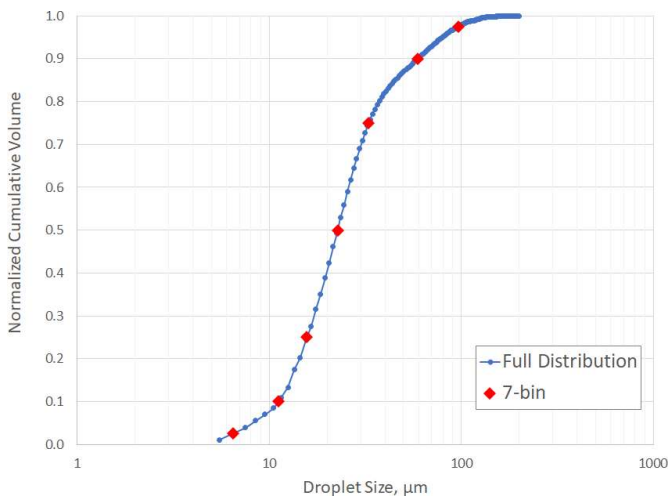| Droplet size [µm]	LWC [%]
6.5	5
11.2	10
15.7	20
22.7	30
32.9	20
59.5	10
96.7	5

Figure 5. The full droplet size distribution of the icing wind tunnel and the 7-bin representation of it.

Liquid water content

The liquid water content (LWC) of the icing wind tunnel was calibrated using a rotating cylinder method [14]. The calibration was conducted with an aluminum tube with a diameter of 30 mm and length of 200 mm at −10 °C for 10 min at the same height as the test wing. The spatial homogeneity of the droplet distribution in the test section has been tested with an ice accretion grid, see Fig. 6. The grid had a size of 630×630 mm and was placed in the center of the test section. The grid elements had a thickness of 3 mm and a depth of 0.10 m. The test was conducted as the test case conditions stated in Tab. 1 at a temperature of −10 °C and a duration of 10 min. Ice thicknesses were measured at the center of each grid element and the LWC was estimated following the icing blade calibration method in ARP5905. For this, a collection efficiency of 0.93 was calculated using LEWICE2D simulations with the aforementioned droplet distribution. Furthermore, an ice density of 800 kg/m³ was assumed [14], though this value may be open for discussion [10].

The result of the LWC spatial homogeneity test from the grid is shown in Fig. 7. The data shows clearly that there is substantial spatial variability of the LWC in the flow field. Values generally decline towards the wall of the tunnel. The highest LWC values are

obtained slightly lower than the middle point of the tunnel. There is an approximately 200×100 mm large section with a relatively low variation of the LWC – which coincides with the location of the test wing.
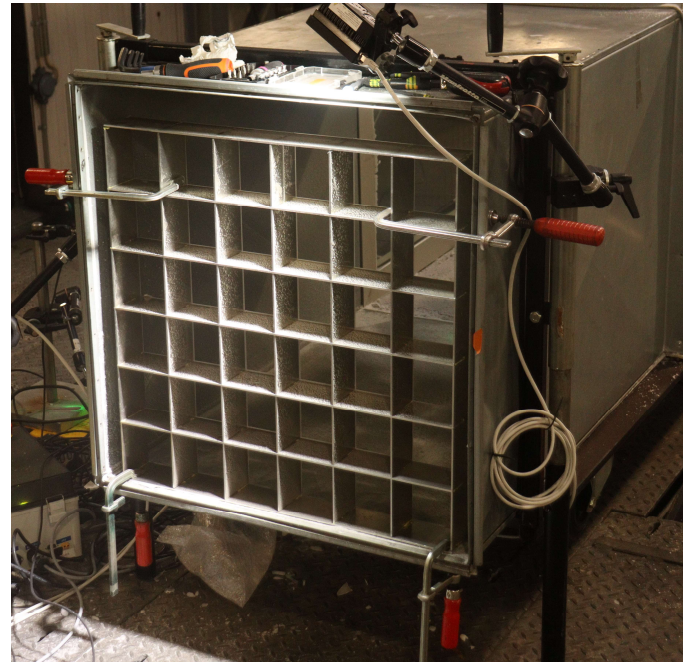

Figure 6. The ice accretion grid is mounted in the test section of the icing wind tunnel.
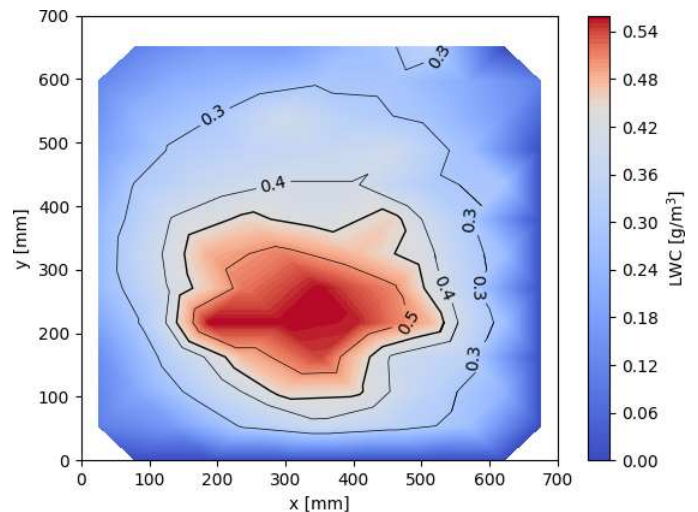

Figure 7. Results of the LWC spatial homogeneity test of the icing wind tunnel. The bold line marks the nominal LWC value of 0.44 g/m³.

Photogrammetry and post-processing

The ice shapes on the removable leading edge were processed with a photogrammetry setup, which was installed in the cold room. The photogrammetry method entails taking a series of pictures of the object of interest and then processing it with a SfM software to generate a 3D model [15, 16]. After ice accretion, the leading edge was removed from the wing, and the ice shapes were spray painted with acrylic white paint using an airbrush pistol – this is done to increase the contrast in the photos and improve photogrammetry results, especially for clear ice (glaze) cases. The paint was given enough time to freeze before the ice shapes were further processed.

Next, a thin layer of fine face powder was applied with a soft brush to further improve contrast. The ice shapes were then placed inside the photogrammetry setup shown in Fig. 8. The setup consists of a rotary table, a lightbox with a green background, a tripod, and Sony A6400 compact camera with 24-megapixel resolution and a Sony E PZ 16–50 mm F3,5–5,6 OSS lens. A series of photos were taken from different angles. The photos were processed with the structure-from-motion software Aigsoft Metashape (version 1.7.1), which generates a 3D model. A more detailed description and validation of this photogrammetry method is planned for the near future. The resulting 3D model output from the SfM method was further processed in Tecplot to obtain the maximum combined cross-section (MCCS). The MCCS represents the outermost extent of the 3D ice shapes [17]. To calculate the MCCS, the ice geometry has been evaluated at 41 equidistant cross-sections. Finally, the ice shapes were weighed on a Precise 500M-2000C scale with 1 mg precision, and caliper measurements of the ice thickness and width are taken.

Figure 8. The photogrammetry setup with the removable leading edge situated on top of the turntable, inside the light box. A camera on a tripod is taking a series of pictures as the turntable rotates the ice shape.

Table 1. Summary of all test case conditions.

Airfoil	RG-15
Span	0.58 m
Chord	0.30 m
Airspeed	25 m/s
Angle of attack	+4°
Liquid water content (LWC)	0.44 g/m³
Mean volume diameter (MVD)	23 microns
Duration	20 min
Static temperature (glaze, mixed, rime)	[−2, −4, −10] °C
Reynolds numbers	[5.7, 5.8, 6.0]×10^5
Relative Humidity	95–100%

Results

Here, the results of the 3D photogrammetry process are shown. First the ice shape data and the 3D models. Then the post-processed MCCS and the estimated ice densities.

Ice shapes

Figures 9–11 show closeups photos of the ice shapes. All ice shapes show a clear presence of ice feathers, which extend on the pressure side to a chord length of ca. 20–30% and on the suction side to ca. 10% in all cases. The rime case in Fig. 11 presents a typical dry rime case with an overall streamlined geometry. The ice color is white and opaque. The mixed ice case in Fig. 10 shows an ice shape that is driven by simultaneous wet and dry ice growth. The ice shape on the leading edge is less streamlined and bulkier but without any clear horn formation. The ice feathers and the base of the ice shape were white, whereas the bulk ice was semi-transparent. The glaze ice chase in Fig. 9 shows smaller ice feathers compared to the other cases and a very amorphous ice shape with a nodular surface structure. The glaze ice was fully transparent.
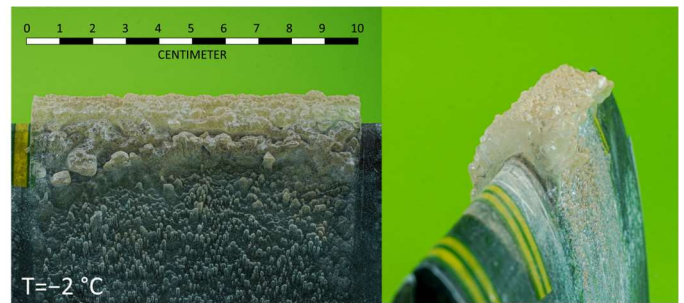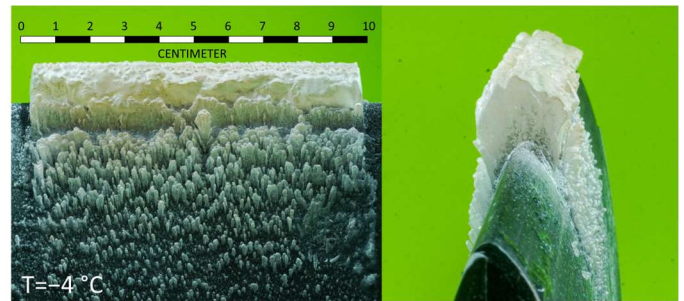

Figure 9. Close-up photo of the glaze ice shape.

Figure 10. Close-up photo of the mixed ice shape.

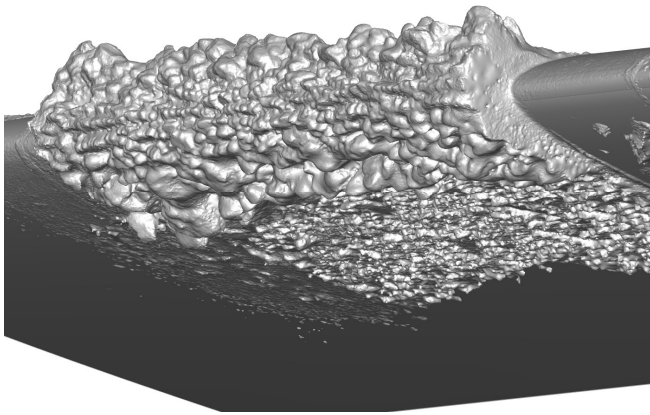Figure 11. Close-up photo of the rime ice shape.

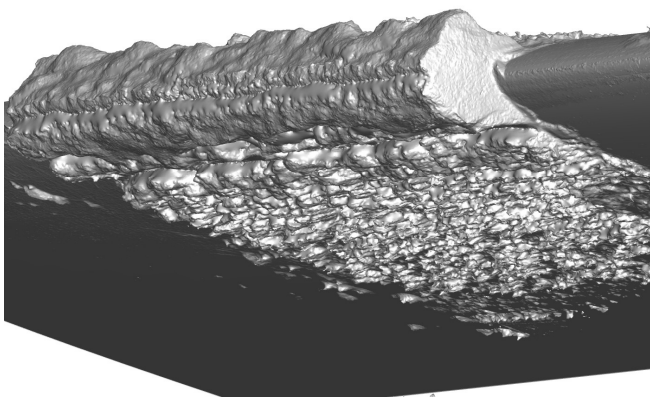Figure 12. 3D model result from the SfM method for glaze ice shape.

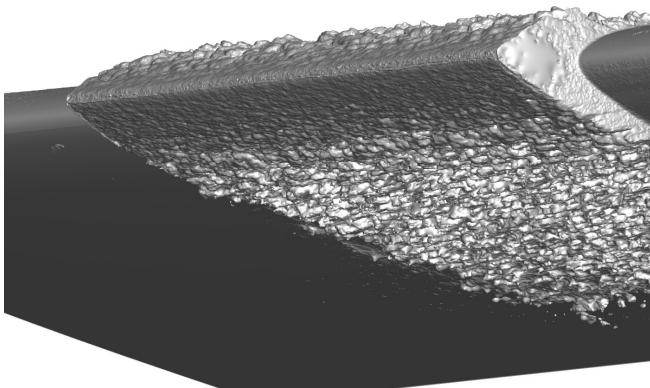Figure 13. 3D model result from the SfM method for mixed ice shape.

Figure 14. 3D model result from the SfM method for rime ice shape.

3D models

The 3D photogrammetry results for the three test cases are shown in Figs. 12–14. Overall, the SfM method is able to capture the geometry with high fidelity and without any significant holes or gaps. The limitations of the resolution can be best observed with the ice feathers. Larger feathers, especially as seen with the rime case in Fig. 14, are captured as distinct features. However, smaller feathers are not well captured and appear as cohesive surface roughness elements. The glaze ice case is the most challenging to digitize, due to the transparency of ice and the challenges of spray painting it, due to the surface wetness). The captured model, in Fig. 12, shows that

the glaze case has been captured well with its nodular surface. The complex surface morphology is successfully represented and there are no large holes in the geometry.

MCCS

The post-processed MCCS results are shown in Figs. 15–17. All three ice shapes are distinctively different from each other. The glaze ice shape shows a bulky ice horn with limited variation between the cross-sections. On the mixed ice shape in Fig. 16, the MCCS method seems to smooth out some of the more detailed features of the ice shape. In particular, around a chord length of ca. 5 mm, some concave features disappear. The MCCS of the rime ice shape shows very little variation along the main ice horn, with more variation downstream in the feather region.
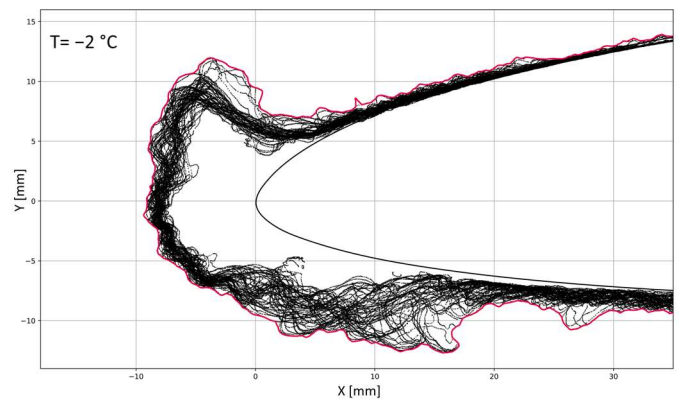

Figure 15. MCCS from 21 cross-sections of the glaze ice shape.
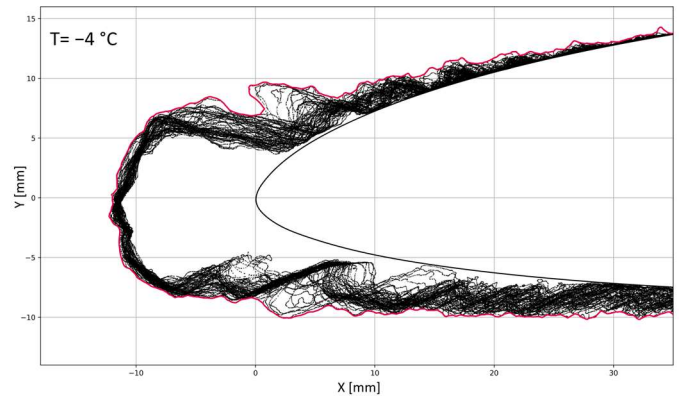

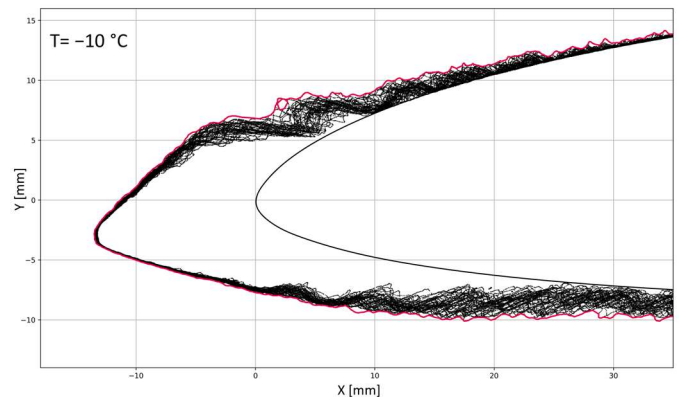Figure 16. MCCS from 21 cross-sections of the mixed ice shape.

Figure 17. MCCS from 21 cross-sections of the rime ice shape.

Ice density

The ice volume is estimated by first calculating the average ice area from the average cross-section area based on five equidistant cross-sections, spaced 1 cm apart on the center of the ice shape. This average ice area is then multiplied by the measured span of the ice to calculate the volume. The ice weight is obtained by the weight difference between the clean and iced removable leading edge. Using the volume and weight, the density is calculated. The results are presented in Tab. 2. The value for glaze is larger than the textbook value for ice density of water, which is 917 kg/m³. This suggests that the accuracy of the method is not sufficiently high yet to calculate the ice density confidently in this way. However, the other values are in a plausible range and the general trend of decreasing ice density at lower temperatures (higher freezing fraction) is also plausible.

Table 3. Estimated ice densities, based on the average of five ice area cross sections, ice shape width, and ice weight.

Rime (−10 °C)	859 kg/m³
Mixed (−4 °C)	898 kg/m³
Glaze (−2 °C)	1142 kg/m³

Discussion

Generating experimental data that are suitable for the validation of numerical methods generally requires high-quality methods and confidence in the experiments. For manned aviation, arguably only a few datasets such datasets exist [7]. We acknowledge that the presented experimental data in this work has several weaknesses and unknowns that limit the validity of the data. However, given that the field of low Reynolds number icing is advancing rapidly, we believe there is a large value in any experiments. Another aspect that may be relevant is the choice of material (PLA) which is different from typical materials used for UAV wing production (e.g. carbon fiber, glass fiber, foam). This may be relevant as it has been shown that material, and heat conductivity in particular, have an impact on ice shape [18].

There are several aspects of the experiments that need to be critically addressed. First of all, the experiments do lack some critical information that would be required for in-depth validation of icing codes. The main missing data here are pressure measurements on the iced airfoil. Such data would allow to more closely match the aerodynamic conditions between the simulations and experiments. Without such measurements, several real-world effects are originating, (wind tunnel walls, mounting side plates, etc.) that are unknown. Furthermore, the density of the ice was measured only with very simplistic methods. It has been shown, that ice density plays an important role in ice shape prediction [7] and there is little available data for ice densities at low-speed ice accretion cases.

Other issues are related to the wind tunnel setup itself. While there have been several studies on the repeatability of this tunnel [10], the presented cases have not been checked for repeatability. There is a possibility that either due to stochastic processes or wind tunnel malfunctions (blocked spray nozzles, flow fluctuations, etc.) the ice shapes are not representative of real-world conditions. Furthermore, there is no very close time link for the calibration of the icing cloud parameters. The calibration of the LWC and the check of the homogeneity of the LWC in the flow has been checked during the same campaign as the tests were done but with a few days in

between. While it is a low likelihood that this would introduce major errors, it remains a potential risk. In particular, the droplet size distribution data is several years old. However, there have not been any relevant changes to the spray bar system, which gives confidence in the distributions.

The novel SfM method to capture the ice shapes with photogrammetry is a risk in itself. The method has not been validated in depth before for icing. However, the method is currently under development with very promising results, also from other fields [16]. The main challenge here lies within the transparency of ice and the difficulty of generating enough contrast for the SfM software to identify a sufficient amount of points – especially on the leading edge. However, a qualitative assessment of the glaze ice case suggests that using the combination of spray paint and powder is sufficient to make the method work. Another key limitation of the method is the resolution. As has been seen with the small ice feathers, there is a limit to how small of features can be resolved with the method. However, we believe that this method is far superior to using hand-tracing methods, significantly cheaper compared to sophisticated laser-scanning methods, and reasonably fast compared to casting methods.

Summary

The objective of this work was to generate an experimental validation dataset for low Reynolds number icing cases based on icing wind tunnel experiments. Three cases were selected, each of which represents typical icing morphology (rime, mixed, glaze). For each case, a 3D model of ice shapes has been generated with a photogrammetry method. Based on this, an MCCS has been generated for each of them. In addition, the approximate ice density was estimated, based on the 3D volume and weight measurements. This data is intended to be used for comparison of icing CFD codes in their ability to predict ice shapes at low-speed cases, as they are common for UAV, UAM, and AAM applications. Further work will focus on refining the methodology and generating more data cases with higher experimental confidence.

Data availability

The experimental data is made available for purposes of validation. The data will be archived in a scientific repository soon and can be accessed via the website of the 2nd AIAA Ice Prediction Workshop (www.icepredictionworkshop.com).

References

[1]   Hann, R., and Johansen, T., *Unsettled Topics in UAV Icing*, SAE International, SAE EDGE Research Report EPR2020008, 2020.

[2]   Hann, R., *Atmospheric Ice Accretions, Aerodynamic Icing Penalties, and Ice Protection Systems on Unmanned Aerial Vehicles*, PhD Thesis NTNU2020:200, Norwegian University of Science and Technology, 2020.

[3]   Gao, M., Hugenholtz, C. H., Fox, T. A., Kucharczyk, M., Barchyn, T. E., and Nesbit, P. R., "Weather constraints on global drone flyability," *Scientific Reports*, 2021, pp. 1–13. https://doi.org/10.1038/s41598-021-91325-w

[4]   Goyal, R., *Urban Air Mobility (UAM) Market Study*, NASA

Report HQ-E-DAA-TN65181, 2018.

[5]   Shahab, H., *Urban Air Mobility (UAM) Market Study*, NASA Report HQ-E-DAA-TN70296, 2019. https://doi.org/10.4324/9781351212991-4

[6]   Hann, R., "UAV Icing: Challenges for computational fluid dynamic (CFD) tools," *International Conference on Computational Fluid Dynamics (ICCFD11)*, 2022.

[7]   Laurendeau, E., Bourgault-Cote, S., Ozcer, I. A., Hann, R., Radenac, E., and Pueyo, A., "Summary from the 1st AIAA Ice Prediction Workshop," *AIAA AVIATION 2022 Forum*. https://doi.org/10.2514/6.2022-3398

[8]   Hann, R., and Müller, N., "Icing Validation Database". DataverseNO, version 1. https://doi.org/doi:10.18710/5XYALW

[9]   Tiihonen, M., Jokela, T., Makkonen, L., and Bluemink, G., "VTT Icing Wind Tunnel 2.0," *Winterwind Conference*, 2016.

[10] Hann, R., "UAV Icing: Ice Accretion Experiments and Validation," *SAE Technical Papers*, 2019, pp. 1–10. https://doi.org/10.4271/2019-01-2037

[11] Jokela, T., Tiihonen, M., and Karlsson, T., "Validation of Droplet Size in the VTT Icing Wind Tunnel Test Section," *Winterwind Conference*, 2019.

[12] Kaikkonen, V. A., Molkoselkä, E. O., and Mäkynen, A. J., "Droplet size distribution and liquid water content monitoring in icing conditions with the ICEMET sensor," *Proc. Int. Workshop on Atmospheric Icing of Structures*, 2019.

[13] Kaikkonen, V. A., Molkoselkä, E. O., and Mäkynen, A. J., "A rotating holographic imager for stationary cloud droplet and ice crystal measurements," *Optical Review*, vol. 27, 2020, pp. 205–216.

[14] SAE International, *ARP5905 Calibration and Acceptance of Icing Wind Tunnels*, Aerospace Recommended Practice ARP5905, 2015.

[15] Westoby, M. J., Brasington, J., Glasser, N. F., Hambrey, M. J., and Reynolds, J. M., "'Structure-from-Motion' photogrammetry: A low-cost, effective tool for geoscience applications," *Geomorphology*, vol. 179, 2012, pp. 300–314.

[16] Betlem, P., Birchall, T., Ogata, K., Park, J., Skurtveit, E., and Senger, K., "Digital drill core models: Structure-from-motion as a tool for the characterisation, orientation, and digital archiving of drill core samples," *Remote Sensing*, vol. 12, 2020, p. 330.

[17] Broeren, A. P., Potapczuk, M. G., Lee, S., Malone, A. M., Paul, B. P., and Woodard, B., "Ice-accretion test results for three large-scale swept-wing models in the NASA Icing Research Tunnel," *8th AIAA Atmospheric and Space Environments Conference*, 2016, p. 3733.

[18] Li, L., Liu, Y., Zhang, Z., and Hu, H., "Effects of thermal conductivity of airframe substrate on the dynamic ice accretion process pertinent to UAS inflight icing phenomena," *International Journal of Heat and Mass Transfer*, vol. 131, 2019, pp. 1184–1195. https://doi.org/10.1016/j.ijheatmasstransfer.2018.11.132

Contact Information

richard.hann@ntnu.no

Acknowledgments

Definitions/Abbreviations

2D	Two dimensional
3D	Three dimensional
AAM	Advanced air mobility
CFD	Computational fluid dynamics
ICEMET	Icing condition evaluation method
IPW	Ice prediction workshop
LWC	Liquid water content
MCCS	Maximum combined cross-section
MVD	Median volume diameter
PLA	Polylactic acid
RPAS	Remotely piloted drone
SfM	Structure from motion
UAM	Urbain air mobility
UAS	Unmanned aerial system
UAV	Unmanned aerial vehicle